Determination of the optimal angle between vertical and inclined piles used for embankment protection during earthquakes

C. Qin
Doctoral student, Faculty of Engineering, Kyushu University, Fukuoka, Japan
H. Hazarika
Professor, Faculty of Engineering, Kyushu University, Fukuoka, Japan
N. Ogawa
Assistant Manager, Construction Solutions Development Department, GIKEN LTD., Tokyo, Japan

ABSTRACT

Vertical piles are commonly used as a traditional reinforcement method to prevent slope failure and have been extensively utilized in numerous cases. Additionally, it has been observed that in earthquake-induced damage, displacement mainly occurs at the pile head, leading to the compromise of the integrity of vertical piles. The authors investigated the effectiveness of using a hybrid countermeasure comprising vertical and inclined micro-piles for highway embankments located on saturated sandy soils through numerical analysis. The findings indicate that relying solely on vertical piles results in significant deformation at the pile head after seismic loading. However, introducing an inclined pile that is securely connected to the vertical pile head provides lateral support to the vertical pile head, thus enhancing the dynamic stability of the hybrid pile system. Nevertheless, determining the optimal angle between the vertical and inclined piles requires further investigation. This study aims not only to identify the most suitable angle between vertical and inclined piles through static analysis but also to extend its focus to dynamic analysis. Comparative analysis suggests that with a fixed length of the inclined pile, the optimal angle under static loading conditions is around 47°, taking into account the dimensions of the highway embankment and the length of the inclined pile. Moreover, in dynamic analyses, the most suitable angle is estimated to be 65°.

Key words: *Dynamic effective stress analysis, Embankment settlement, Highway embankment, Hybrid retrofitting technique, Liquefaction*

1. Introduction

The pursuit of Sustainable Development Goal 11, which aims to create inclusive, safe, resilient, and sustainable cities, underscores the importance of reducing disaster exposure and increasing resilience. Within this framework, highways emerge as vital lifelines, facilitating the flow of essential rescue and relief resources during calamities. However, the resilience of these critical pathways is compromised in Japan, where many highway embankments built on soft soil are aging and increasingly vulnerable to natural disasters. A case in point is the damage observed to the highway embankment and retaining walls along the Kyushu Expressway near Mashiki town during the 2016 Kumamoto earthquakes, as documented (Hazarika et al. 2017).

In response to these challenges, a novel, cost-effective hybrid type reinforcement comprising vertical and inclined piles was introduced using 1g shaking table tests (Qin et al. 2024). This reinforcement's practicality has been validated using data from 1g shaking table tests and simulated using the dimensions of 1g shaking table tests, thus demonstrating the validity of the numerical model (Hazarika et al. 2022). The effectiveness of inclined piles within a liquefiable sandy layer was investigated,

revealing their superior performance over vertical piles, as demonstrated in studies (Wang and Orense 2020, Wang and Orense 2022, Wang and Orense 2023). Research by (Mc. Manus, Turner and Charton 2005) and (Shahrour and Juran 2004) has shown that inclined piles contribute to reducing soil deformation and preventing the accumulation of excess pore water pressure, due to the increased lateral stiffness they provide.

In order to further investigate the effectiveness of the inclined pile in this reinforcement, simulations were conducted using real dimensions and seismic loading recorded from the 2016 Kumamoto Earthquakes (Qin et al. 2022). This study primarily relied on the lateral forces calculated under static loads and then identified the most suitable reinforcement under dynamic loadings by selecting several cases with different angles between vertical and inclined piles.

2. Static lateral force on pile head.

To investigate the angle between vertical and inclined piles, it is beneficial to examine the lateral force provided by the inclined piles to the pile head. Therefore, using the principle of superposition to calculate the vertical stress acting on the inclined piles and integrating to obtain the total force, the lateral force acting on the pile head can be determined by decomposing the force.

2.1. Vertical stress on the inclined piles

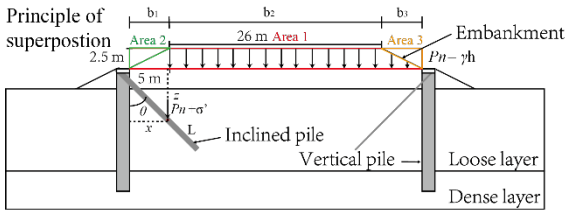

Fig. 1 Vertical stress increment on inclined piles calculated using Principle of superposition.

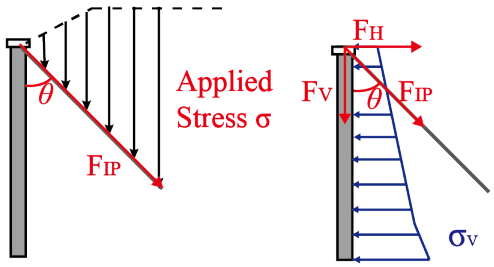

Fig. 2 Horizontal force on inclined piles.

Fig. 1 illustrates the stress acting on the inclined pile by considering the highway embankment load and the effective stress of the loose layer. By utilizing the principle of superposition, the total force (F_{IP}) acting on the inclined pile can be calculated. The formulas 1-13 are as follows:

$$p_n = \gamma_{embankment} \cdot h \tag{1}$$

$$\sigma_z = \sigma_{z1} - \sigma_{z2} - \sigma_{z3} \tag{2}$$

$$\sigma_{z1} = \frac{p_n}{\pi}\left[\tan^{-1}\left(\frac{m_1}{n_1}\right) - \tan^{-1}\left(\frac{m_1-1}{n_1}\right) + \frac{m_1 n_1}{n_1^2+m_1^2} - \frac{n_1(m_1-1)}{n_1^2+(m_1-1)^2}\right] \tag{3}$$

$$\sigma_{z2} = \frac{p_n}{\pi}\left\{m_2\left[\tan^{-1}\left(\frac{m_2}{n_2}\right) - \tan^{-1}\left(\frac{m_2-1}{n_2}\right)\right] - \frac{n_2(m_2-1)}{n_2^2+(m_2-1)^2}\right\} \tag{4}$$

$$\sigma_{z3} = \frac{p_n}{\pi}\left\{m_3\left[\tan^{-1}\left(\frac{m_3}{n_3}\right) - \tan^{-1}\left(\frac{m_3-1}{n_3}\right)\right] - \frac{n_3(m_3-1)}{n_3^2+(m_3-1)^2}\right\} \tag{5}$$

$$m_1 = \frac{x}{b_1+b_2+b_3} \tag{6}$$

$$n_1 = \frac{z}{b_1+b_2+b_3} \tag{7}$$

$$m_2 = \frac{-x+b_1}{b_1} \tag{8}$$

$$n_2 = \frac{z}{b_1} \tag{9}$$

$$m_3 = \frac{x-b_1-b_2}{b_3} \tag{10}$$

$$n_3 = \frac{z}{b_3} \tag{11}$$

$$\sigma' = \gamma_{Loose\ layer} \cdot H_{Loose\ layer} \tag{12}$$

$$F_{IP} = \int_x^O \mu(\sigma_z + \sigma')\, dx \tag{13}$$

2.2. Decomposition of force

Fig. 2 shows the horizontal force (F_H) acting on the pile head. By applying Eq. 14, the forces can be decomposed to calculate the applied force (F_{IP}) acting on the pile head.

$$F_H = \sin\theta \cdot F_{IP} \tag{14}$$

2.3. Relationship between lateral force and inclination angle

To calculate the lateral force at various angles, a brute force method was employed to input angles (θ) ranging from 0 to 90° at 0.01° intervals into the aforementioned formula. The results of these calculations are displayed in

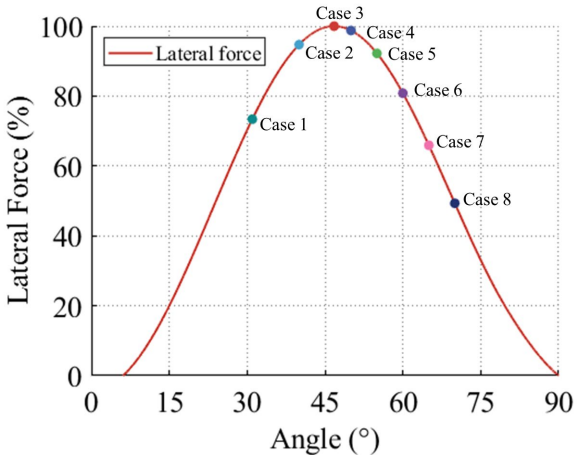

Fig. 3 Lateral force calculated by different angles between vertical and inclined piles.

Table 1. Numerical models with different configurations

	Angle between vertical and inclined piles (°)
Case 0	No
Case 1	31
Case 2	40
Case 3	46.75
Case 4	50
Case 5	55
Case 6	60
Case 7	65
Case 8	69

Eight angles were selected as comparative cases based on Fig. 3, and their configurations with the inserted angles are presented in Table 1. Based on static analysis, it revealed that an angle of 46.75 ° provided the maximum lateral force, which is considered as Case 3 for further discussion. Additionally, Case 1 was initially intended to use an angle of 30°, but for avoiding excessively small elements in finite element analysis, it was adjusted to 31°. Similarly, Case 8 was adjusted to 69° for the same reason.

3. Numerical approach

3.1. Numerical model and boundary conditions

Fig. 4 illustrates a 10-meter thick dense sandy layer, upon which lies a 10-meter thick saturated sandy layer, which has liquefaction potential. A symmetrical embankment, 5 meters in height with a road surface width of 26 meters and a slope of 1:2, is constructed on top of this liquefiable layer. For the embankment and foundation soil, a cyclic elasto-plastic model was adopted as the constitutive law. The embankment was treated as the dry element, and the foundation was treated as the saturated element. The properties of foundation and embankment materials were referred (Qin et al. 2022). In all cases, vertical piles with a diameter of 1.5 meters and an insertion depth of 15 meters are included. Additionally, in cases where hybrid type reinforcement is used, inclined piles with a diameter of 0.2 meters and a length of 14 meters are connected on top of the existing vertical piles. To accurately represent the volume of the pile, the model employed hybrid beam elements for the vertical pile, which integrated conventional beam elements with elastic solid elements (Zhang, Okawa and Kimura 2008). Joint elements were placed at every interface between the soil and the piles to ensure uniform horizontal displacements. The base of the model was made rigid to simulate a solid foundation, while a drainage boundary was established at the ground's surface to match the water table with the

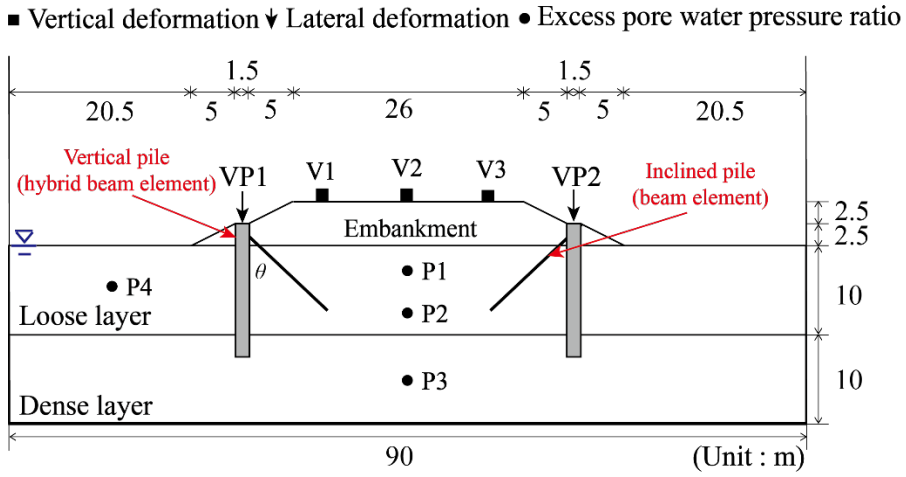

Fig. 4 Finite element model for Case 3 and selected node and elements for discussion.

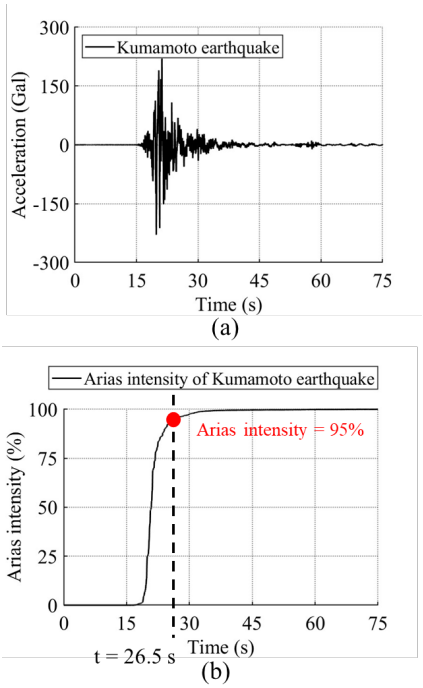

Fig. 5 Seismic input motion applied in analysis (Strong-motion Seismograph Networks): (a) time history and (b) arias intensity.

surface level. To minimize boundary effects, the ground model was extensively expanded on both sides in the X direction, with an extension length of 50 times the size of the model, which is 4500 meters. An incremental time interval of 0.001 s was employed, with the parameters β and γ set to 0.3025 and 0.6, respectively, in the Newmark integration method to ensure numerical stability.

3.2. Input motion

This model is based on the simplified analysis of the north-south oriented highway embankment damaged in Mashiki town during the 2016 Kumamoto Earthquakes. Therefore, in selecting the seismic loadings, the closest seismic station (KMMH16 station) in Kumamoto Prefecture, Japan was chosen. As a result, seismic loadings from approximately 200 meters underground in the east-west direction were selected. Fig. 5 (a) shows the time history of seismic loading (75 s) used in all the cases. Due to the dissipation of water pressure after liquefaction, the embankment will experience a certain level of settlement. Therefore, after 75 seconds of seismic loading, an additional 3600 seconds of gravity loading were applied to ensure complete dissipation of water pressure within the model.

Arias intensity (I_A) is calculated by summing the squared acceleration values obtained from dynamic recordings using Eq. 15 (Arias 1970). This parameter is considered a reliable indicator for describing the level of earthquake shaking that can lead to embankment failure, as identified by Arias, 1970. The equation is derived as follows:

$$I_A = \frac{\pi}{2g}\int_0^{T_d} a(t)^2 dt \tag{15}$$

In the equation, g represents the acceleration due to gravity, and T_d signifies the duration of the ground motion recording. The Arias intensity for the input motion is illustrated in Fig. 5(b). At the 26.5th second, the Arias intensity has reached 95%, making it an appropriate time point for discussing the distribution of excess pore water pressure ratio (R_u) in all models.

4. Results and discussions

Based on the comparison of the representative results from the vertical pile only supported and hybrid-reinforced cases, Therefore, the deformed configuration, time histories of settlement, time histories of pile heads deformation, distribution of excess pore water pressure ratio and time histories of excess pore water pressure ratio in the nice cases are examined.

4.1. Deformed configuration of whole model

Fig. 6 presents a case with only vertical piles, where the black lines represent the condition before the seismic and gravitational loadings, and the red lines indicate the deformation after these loadings. To emphasize the pile deformations, they are highlighted with blue color, clearly showing the seismic deformation. The settlement of the embankment cannot be observed from the macroscopic image and is discussed in subsequent sections along with

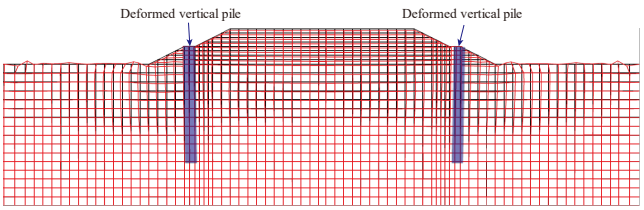

Fig. 6 Deformed configuration of Case 0 (Vertical piles supported embankment) at the end of the simulation (black line: before shaking; red line: after shaking).

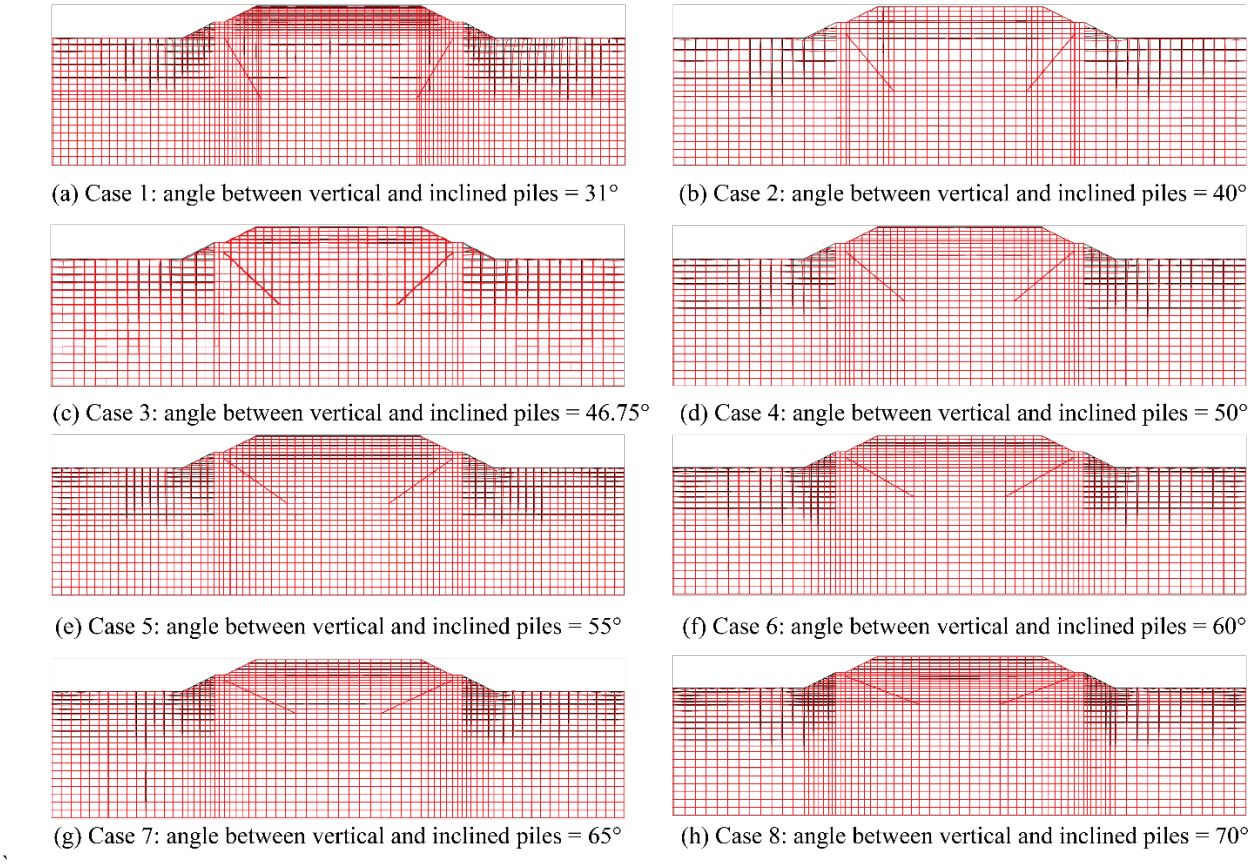

Fig. 7 Deformed configuration of 8 cases (hybrid type reinforcement using different angles) at the end of the simulation (black line: before shaking; red line: after shaking).

embankment settlement and pile head deformations. Fig. 7 displays 8 cases using hybrid type reinforcement, where regardless of the angle, the embankment and loose layer between the vertical piles did not exhibit significant damage, with most damage occurring at the feet of the slope.

4.2. Settlement of embankment

Fig. 8 illustrates the vertical deformations at the embankment surface (at V2) for traditional reinforcement alongside eight varied configurations of hybrid type reinforcements. The positions of points V1, V2, and V3 are indicated in Fig. 4. In Case 0 using traditional reinforcement, vertical deformation (settlement) continued to occur, still increasing at 200 seconds. In contrast, with the hybrid type reinforcement, there was no significant increase in settlement after the earthquake loading ceased. It was observed that, under the hybrid type reinforcement, the magnitude of settlement was restrained to within 5 cm and reduced to less than 20% compared to the traditional method (around 25 cm). To better compare the impact of angles on settlement, Fig. 9 exclusively discusses the residual settlement for the hybrid type reinforcements. Fig. 9 is based on the largest vertical deformation among the eight cases, converted into

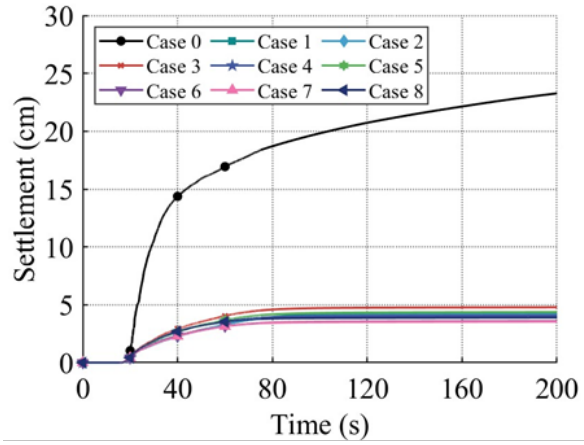

Fig. 8 Time histories of settlement at V2 on the embankment surface for traditional reinforcement and eight different configurations of hybrid type reinforcements

percentages to more effectively highlight the outcomes in each case. Most notably, the settlement at the middle line (V2) of the embankment, as shown in Fig. 9(b), was largest in Case 3, which was identified in static analysis as having the most optimal angle. Conversely, the cases with angles of 60° and 65° experienced the least settlement. Additionally, when observing the settlement on both left and right sides (V1 and V3) of the embankment, Case 7 (angle = 65°) also resulted in the minimal settlement. Therefore, considering the aspect of embankment deformation, Case 7 demonstrates the best performance during earthquake loading.

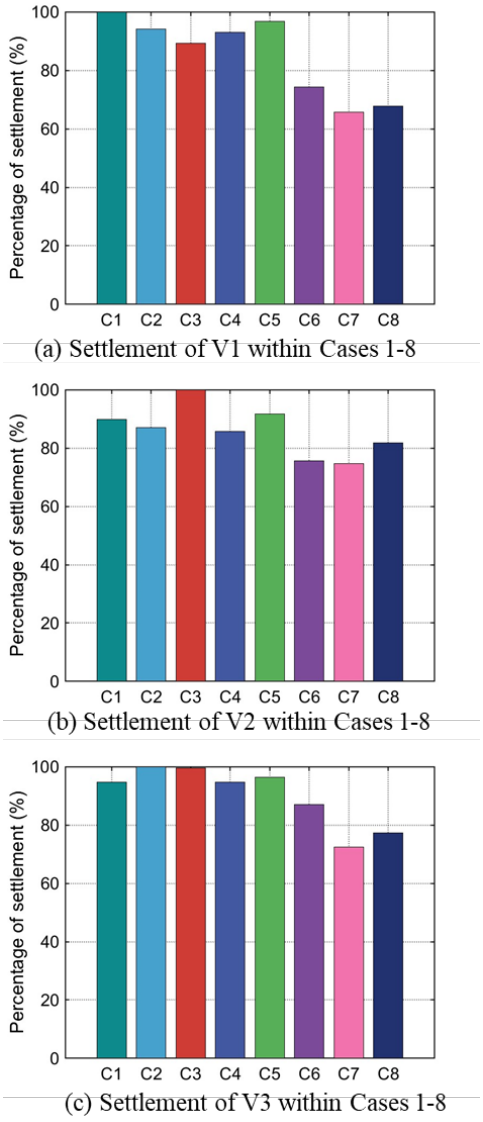

Fig. 9 Percentage of settlement at 3 points (V1, V2 and V3) on the embankment surface for eight different configurations of hybrid type reinforcements: (a) V1, (b) V2 and (c) V3.

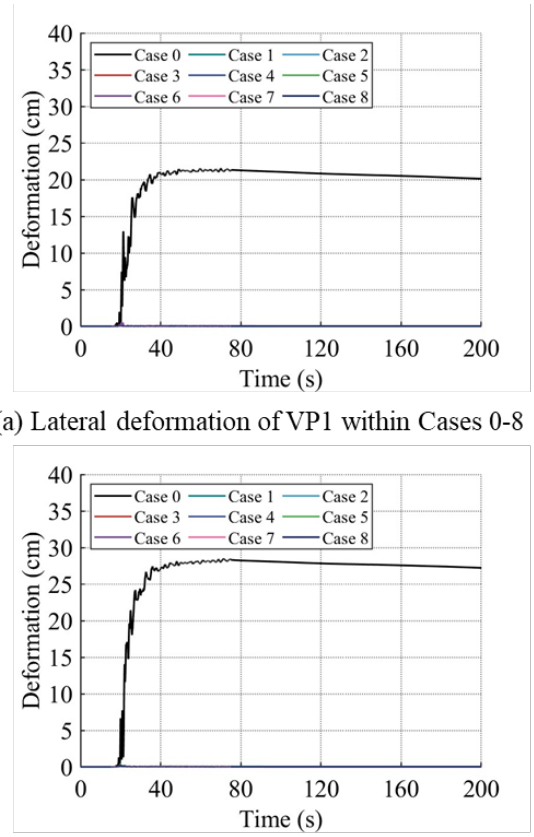

Fig. 10 Time histories of lateral deformation at two vertical piles on the embankment slopes for traditional reinforcement and eight different configurations of hybrid type reinforcements: (a) VP1 and (b) VP2

4.3. Deformation of pile heads

Fig. 10 presents the time histories of lateral deformation observed at two vertical piles located on the embankment slopes, comparing the outcomes between traditional reinforcement methods and eight distinct configurations of hybrid type reinforcements. Fig. 10(a) mentions the lateral deformation at vertical pile VP1, while Fig. 10(b) shows similar deformations at vertical pile VP2. In the traditional reinforcement method, significant deformation occurred at the pile heads, with lateral displacement of around 20 cm on the left side and

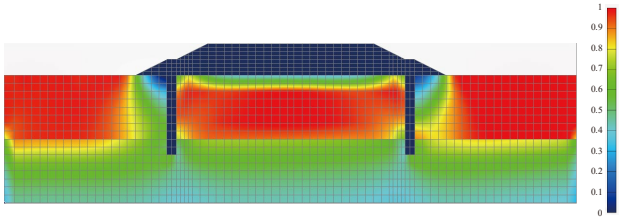

Fig. 11 Distribution of excess pore water pressure ratio (Ru) at the 26.5th of input motion for Case 0.

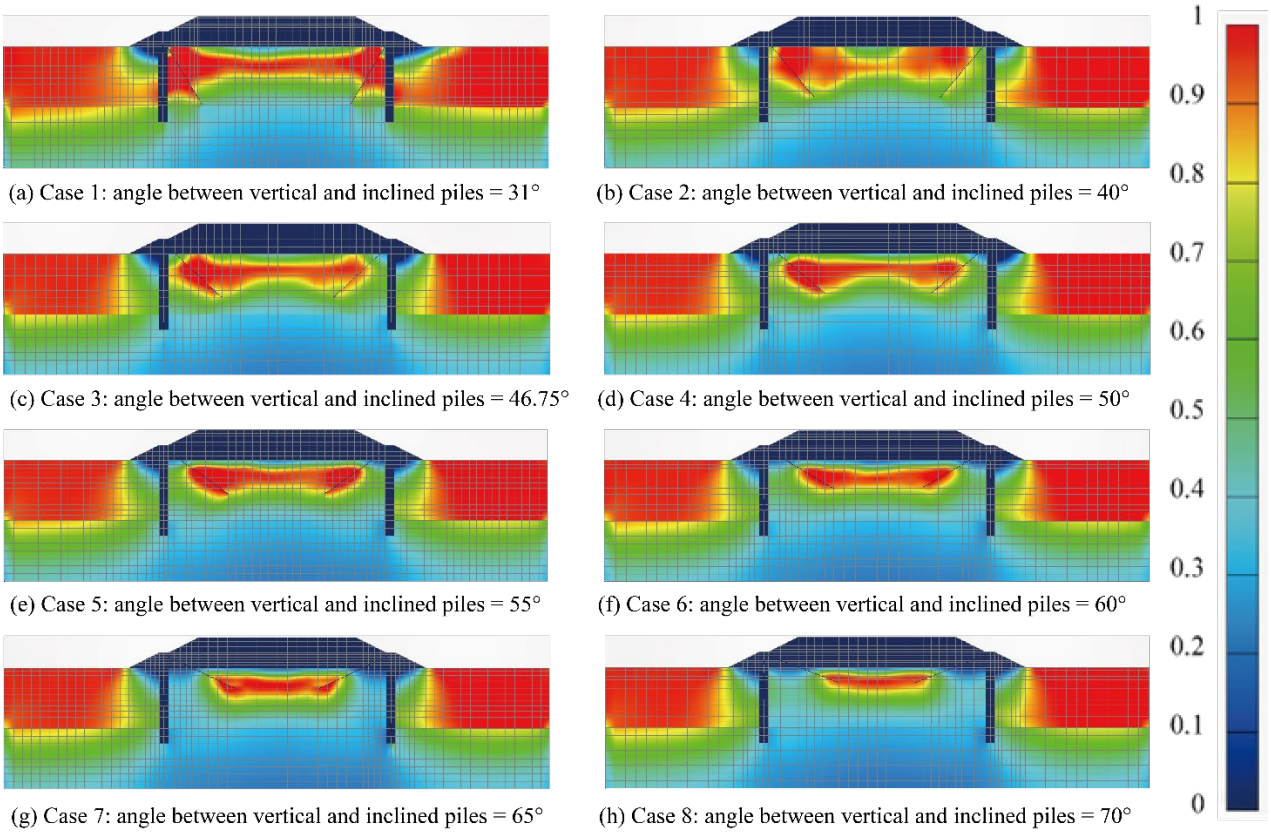

Fig. 12 Distribution of excess pore water pressure ratio (Ru) at the 26.5th of input motion: (a) Case 1; (b) Case 2; (c) Case 3; (d) Case 4; (e) Case 5; (f) Case 6; (g) Case 7; (h) Case 8.

around 27 cm on the right side. However, when inclined piles were utilized, the displacement of the pile heads was reduced to an almost imperceptible level, indicating that lateral tensile forces can effectively mitigate deformation at the pile heads.

4.4. Excess pore water pressure ratio (R_u)

Fig. 11 shows the distribution of excess pore water pressure ratio for the traditional reinforcement (Case 0) at the 26.5th of input motion. The red area indicates that the pore water pressure ratio has reached 1.0, indicating that the area is completely replaced by pore water pressure, leading to a loss of effective stress. In Case 0, the weak soil layer at the bottom of the embankment and the soil in the free field have reached a liquefaction state, rendering them incapable of providing effective support and lateral constraint for the highway embankment.

Fig. 12 illustrates the excess pore water pressure ratio distribution at 26.5th second for 8 different configurations of hybrid type reinforcements. The criteria used for identification in Fig. 12 are consistent with Fig. 11. In Cases 1 and 2, the soil near the inclined piles experienced widespread liquefaction, while in the remaining cases, liquefaction was mainly concentrated in the lower part of the inclined piles and the area between the two inclined piles. In terms of liquefaction condition, Case 7 exhibited the smallest liquefied area.

Fig. 13 presents the time histories of the excess pore water pressure ratio (R_u) observed under two different reinforcement strategies: traditional reinforcement and eight varied hybrid reinforcement configurations. The point locations are referred to Fig. 4. The data shown in Fig. 13(a) is derived from P1, where in all cases, liquefaction occurred at the 20th second, followed by varying rates of dissipation of excess pore water pressure depending on the different configurations of hybrid type reinforcement. Meanwhile, in Fig. 13(b), in the case of using hybrid type reinforcement, the excess pore water pressure ratios for P2 remained within the range of approximately 0.6, without reaching liquefaction. Therefore, the insertion of inclined piles has shown a reinforcing effect on the liquefaction tendency of the lower soil layers. P3 is located in the dense layer, and except for a significant increase of 0.7 in the case of

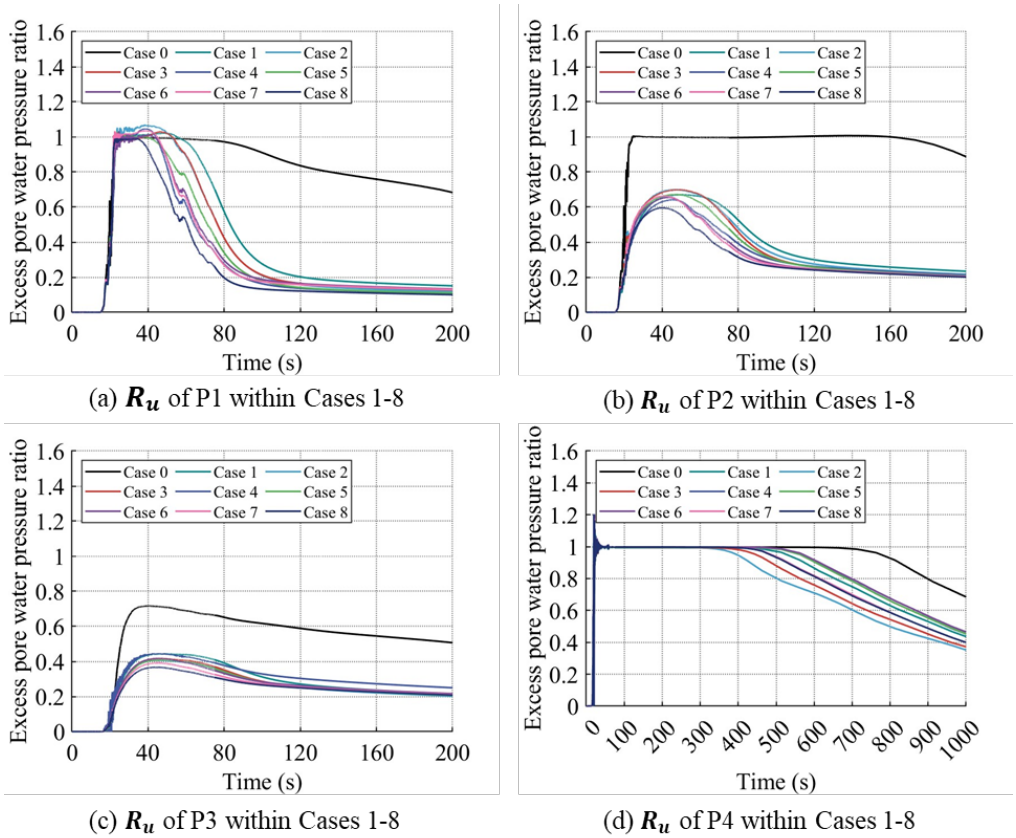

Fig. 13 Time histories of excess pore water pressure ratio (R_u) for traditional reinforcement and eight different configurations of hybrid type reinforcements: (a) P1, (b) P2, (c) P3 and (d) P4.

traditional reinforcement, the excess pore water pressure ratios remained within the range of 0.4. P4 is situated in a free field, and in all cases, it took at least 350 seconds for the process of excess pore water pressure dissipation to occur, indicating that the free field remains in a state of long-term effective stress loss during dynamic simulation.

5. Conclusions

The simulation outcomes reveal that highway embankments reinforced with hybrid type reinforcement exhibit superior settlement reduction capabilities when subjected to earthquake loading. This enhancement is achieved by integrating inclined piles with traditional reinforcement methods, which accomplishes two main objectives: it minimizes pile head deformation and controls the rise of water pressure within the liquefiable layer beneath the embankment during seismic loadings.

To further assess the structural stability, examining the effects of various pile insertion angles is crucial. Static load analyses point that an insertion angle of 46.75° maximizes the lateral restraint force exerted on the pile head. However, seismic activities can induce liquefaction in susceptible layers, affecting the soil's ability to provide the anticipated frictional resistance. Specifically, Case 3 demonstrates a significant liquefaction area in the loose layer under the highway embankment, diminishing the soil's supportive capacity.

Focusing on excess pore water pressure ratio distribution indicates that Case 8 experiences the least liquefaction. This discrepancy arises because, despite Case 8 reduced liquefaction area, the lateral restraint force it generates is insufficient for adequate support. Nonetheless, when analyzing settlement, the hybrid type reinforcement with a 65° insertion angle emerges as most effective in minimizing settlement.

Consequently, hybrid type reinforcement with angle between vertical and inclined piles (65°) emerges as the optimal reinforcement, balancing between minimizing liquefaction and providing effective lateral support.

6. Acknowledgements

This study received financial support from the Nippon Expressway Company Limited (NEXCO) and its affiliated entities. Additionally, the Kyushu Regional

Management Service Association in Fukuoka contributed funding towards a portion of this research. Furthermore, the lead author is grateful for the backing received from JST SPRING (JPMJSP2136).

References

Arias, A., 1970. A measure of earthquake intensity. MIT Press: Cambridge, MA**,** pp. 438–483.

Hazarika, H., et al., 2017. Geotechnical damage due to the 2016 Kumamoto Earthquake and future challenges. Lowland Technology International, 19**,** pp. 203-218.

Hazarika, H., et al., 2022. Hybrid Type Reinforcement of Highway Embankment Against Earthquake Induced Damage. Proceedings of the 4th International Conference on Performance Based Design in Earthquake Geotechnical Engineering (Beijing 2022)**,** pp. 472-499. Cham.

Mc. Manus, K., et al. 2005. Inclined reinforcement to prevent soil liquefaction. In *Proceedings of the New Zealand Society for Earthquake Engineering Conference*, 523-533. Citeseer.

Qin, C., et al., 2022. Numerical Simulation of Seismic Performance of Road Embankment Improved with Hybrid Type Steel Pile Reinforcement. Proceedings of the 4th International Conference on Performance Based Design in Earthquake Geotechnical Engineering (Beijing 2022)**,** pp. 1332-1339. Cham.

Qin, C. J., et al., 2024. Seismic behavior of highway embankment reinforced with remedial countermeasures on saturated loose sandy layer. Transportation Geotechnics, 45**,** pp. 101183.

Shahrour, I. & Juran, I., 2004. Seismic behaviour of micropile systems. Proceedings of the Institution of Civil Engineers - Ground Improvement, 8**,** pp. 109-120.

Wang, Y. & Orense, R. P., 2020. Numerical analysis of seismic performance of inclined piles in liquefiable sands. Soil Dynamics and Earthquake Engineering, 139**,** pp. 106274.

Wang, Y. & Orense, R. P., 2022. Consideration of batter angle in pseudo-static analyses of pile foundations. Computers and Geotechnics, 147**,** pp. 104767.

Wang, Y. & Orense, R. P., 2023. Numerical Investigation of Inclined Piles under Liquefaction-Induced Lateral Spreading. Geotechnics, 3**,** pp. 320-346.

Zhang, F., et al., 2008. Centrifuge model test on dynamic behavior of group-pile foundation with inclined piles and its numerical simulation. Frontiers of Structural and Civil Engineering, 2**,** pp. 233-241.